IOP Publishing | Royal Swedish Academy of Sciences Physica Scripta

Phys. Scr. **91** (2016) 054001 (9pp) doi:10.1088/0031-8949/91/5/054001

Manipulation of ultracold atoms using double-loop microtraps

W A van Wijngaarden, B Jian and A Mouraviev

Physics & Astronomy Deptartment, Petrie Bldg., York University, 4700 Keele St., Toronto, Ontario, M3J 1P3, Canada

E-mail: wlaser@yorku.ca

Received 15 December 2015, revised 23 February 2016
Accepted for publication 9 March 2016
Published 13 April 2016

Abstract

Ultracold atoms created using microtraps are being used in an increasing number of diverse applications. This paper reviews the double-loop microtrap which consists of two concentric circular wire loops carrying oppositely oriented currents. This generates a magnetic field configuration that traps a magnetic dipole in three-dimensions. The position of the trapped atoms relative to the atom chip surface containing the microwire loops, can be precisely controlled by applying different currents in the two loops or alternatively using a so called bias magnetic field oriented perpendicular to the chip surface. Double-loop microtraps can be daisy chained in series to create a one- or two-dimensional microtrap array. Experiments that have demonstrated a double-loop microtrap array are discussed. Future possibilities are presented as to how atoms can be transferred between adjacent microtraps as well as the use of an additional micro sized Ioffe coil to create a trap having a nonzero magnetic field minimum to reduce atom loss by suppressing Majorana transitions.

Keywords: ultracold atoms, atom microtrap, laser cooling

(Some figures may appear in colour only in the online journal)

1. Introduction

Enormous progress has occurred during the past two decades in the field of ultracold atom research [1]. Ultracold atoms are essential for studying Bose–Einstein condensates (BEC) [2–4] and degenerate fermi gases [5]. Transitions observed using ultracold atoms have negligible Doppler broadening making them ideal for improved frequency standards and atomic clocks [6]. An interferometric measurement of the recoil velocity when an ultracold Cs or ^{87}Rb atom absorbed a photon [7, 8] resulted in a value of the fine structure constant with an uncertainty of less than 1 ppb in agreement with the result obtained from the electron g-2 experiment [9]. Ultracold atoms have been used to precisely measure a transition's natural linewidth to yield the radiative lifetime of an excited state to 0.3% accuracy [10] stringently testing many body perturbation theory [11].

The production of ultracold atoms originally required macroscopic magnetic coils having currents as high as hundreds of amps to tightly confine the atoms. Turning off such currents in times of milliseconds to avoid damage to power supplies necessitated the construction of electronic circuits to divert currents into dummy load resistors. There has been considerable progress to facilitate the production of ultracold atoms using traps created by the magnetic fields generated with micron sized wires [12–14]. Magnetic microtraps have larger field gradients than macroscopic traps and use orders of magnitude less current. Diverse applications have been reported in BEC production and manipulation [15, 16], surface sensing [17], atom interferometry [18] and quantum entanglement [19], to name a few. Magnetic ring traps are being developed [20] to fabricate a Sagnac atom interferometer [21].

There is growing interest in creating arrays of ultracold atoms to eventually study quantum information processing [22–24]. Considerable work has been done with optical lattices formed when two counterpropagating laser beams create a standing wave [25]. Alternatively, an array of optical traps can be created using microlenses to generate multiple infrared laser foci [26, 27]. Arrays of magnetic microtraps can be created using the permanent field of a surface magnetic film

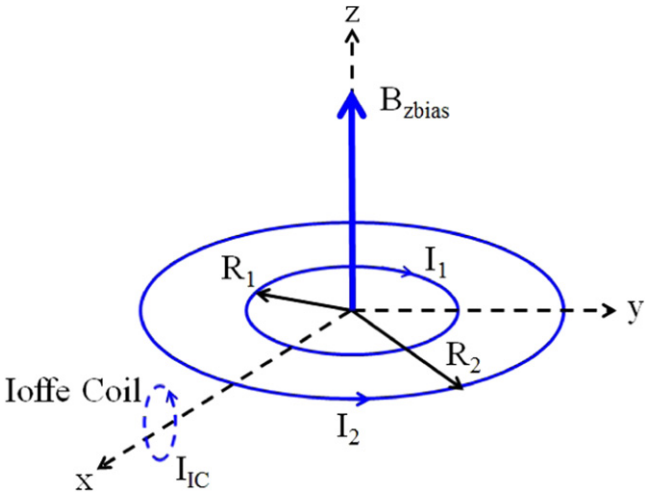

Figure 1. Double-loop microtrap configuration with Ioffe coil. The microtrap consists of two concentric coils having radii R_1 and R_2, carrying currents I_1 and I_2 respectively. A bias field $B_{\rm zbias}$ may be applied along the z-direction perpendicular to the $x-y$ plane that contains the microwire loops. An Ioffe coil having a radius $R_{\rm IC}$ and current $I_{\rm IC}$ is centered about position $(x_{\rm IC}, 0, z_{\rm IC})$. The direction of $I_{\rm IC}$ is such that a positive current generates a field in the $+x$-direction. The Ioffe Coil perturbs the magnetic field generated by the double-loop trap so that the trap minimum has a nonzero field to prevent loss of atoms due to spin flips as is discussed in the text.

[28, 29]. A limitation of such arrays is the difficulty to modify the potential of an individual microtrap.

This paper reviews the so called double-loop microtrap consisting of two concentric loops carrying opposite currents [30–32]. This trap can be readily daisy chained in series to create a one- or two-dimensional microtrap array. The microwire loop currents can also be adjusted to modify the position of the atom clouds relative to the atom chip surface which is critical for studying interactions with the surface. The theory of the double-loop microtrap is discussed first and how it can be used to create a microtrap array. Next, a review of experiments that have demonstrated several methods to load atoms into a double-loop microtrap array is given. Finally, conclusions and future prospects for these microtraps are presented.

2. Theory of double-loop microtrap

The double-loop microtrap is illustrated in figure 1. It is composed of two concentric wire loops of radii R_1 and R_2 in the $x-y$ plane carrying oppositely oriented currents I_1 and I_2, respectively. A bias field $B_{\rm zbias}$ may be applied along the z-direction to shift the trap minimum relative to the chip surface. Bias fields can also be applied in the x- and y-directions to adjust the transverse position of the trap [33]. For simplicity, we first consider the case of an equal current double-loop trap operated with a zero bias field to show how this configuration creates an atom trap. The magnetic field along the

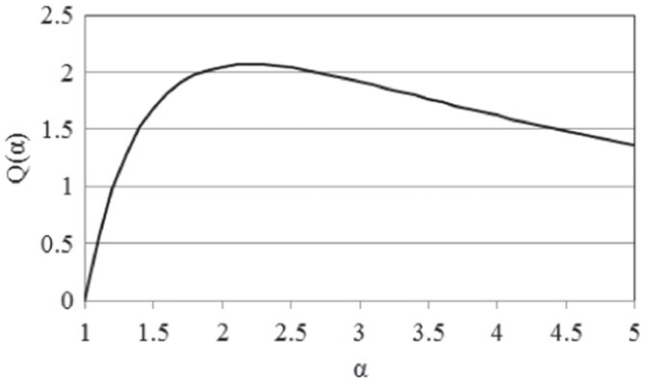

Figure 2. Plot of numerical factor Q versus α.

z-direction is given by the following expression

$$\vec{B}(0, 0, z) = 2\pi B_o\left[\frac{\alpha^2 R_1^3}{(\alpha^2 R_1^2 + z^2)^{3/2}} - \frac{R_1^3}{(R_1^2 + z^2)^{3/2}}\right]\hat{z}, \quad (1)$$

where $\alpha = R_2/R_1$, $B_o = \frac{\mu_o I}{4\pi R_1}$ and μ_o is the permeability of free space. The magnetic field is zero at position

$$z_{\rm min} = \frac{\alpha^{2/3}}{\sqrt{1 + \alpha^{2/3}}} R_1. \quad (2)$$

The field gradient at $z_{\rm min}$ has the value

$$\frac{{\rm d}B_z}{{\rm d}z}(0, 0, z_{\rm min}) = Q(\alpha)\frac{B_o}{R_1}, \quad (3)$$

where

$$Q(\alpha) = 6\pi\left[\frac{(\alpha^{2/3} - 1)(\alpha^{2/3} + 1)^3}{\alpha^{2/3}(\alpha^{4/3} + \alpha^{2/3} + 1)^{5/2}}\right]. \quad (4)$$

$Q(\alpha)$ is a numerical factor that is plotted in figure 2. An atom having a magnetic dipole moment is trapped if the magnetic field gradient force exceeds the gravitational force.

$$g_F m_F \mu_{\rm B}\frac{{\rm d}B_z}{{\rm d}z} \gg Mg. \quad (5)$$

Here, g_F is the Landé g-factor for an atom in the $|F, m_F\rangle$ hyperfine level where F is the sum of the nuclear spin and electronic angular momentum and m_F is its azimuthal component. $\mu_{\rm B}$ is the Bohr magneton, g is the gravitational acceleration and M is the atomic mass. Substituting the expression for the field gradient yields the following

$$\frac{I\,({\rm Amps})}{R_1\,({\rm meter})^2} \gg 1.77 \times 10^4 \frac{M\,({\rm amu})}{g_F m_F Q(\alpha)}. \quad (6)$$

We now consider a ^{87}Rb atom occupying its ground state $|F = 2, m_F = 2\rangle$ hyperfine sublevel for the case when $\alpha = 1.4$. The current required to trap the atom exceeds several hundred amps if the inner coil radius $R_1 = 1$ cm. This current can only be achieved using a macroscopic solenoid having many wire windings. However, if $R_1 = 100\,\mu$m, the

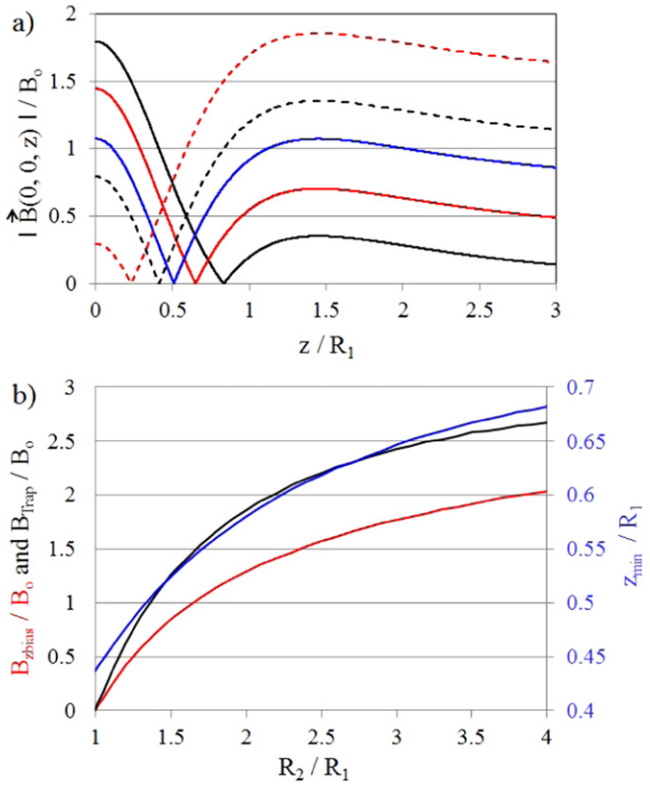

Figure 3. Equal current double-loop microtrap. (a) shows the magnitude of the magnetic field as a function of the distance z from the chip surface at $z = 0$ for the values B_{zbias}/B_o of 0 (solid black), 0.35 (solid red), 0.72 (solid blue), 1 (black dash) and 1.5 (red dash) for the case when $R_2 = 1.4R_1$. (b) shows the dependence of B_{zbias}/B_o (red) that symmetrizes the trap along the z-direction, the trap depth (black) and position of the microtrap along the z-axis (blue) as a function of R_2/R_1.

required current is four orders of magnitude smaller and a single wire double-loop microtrap is possible.

The magnetic field generated by the double-loop microtrap along the z-axis is plotted in figure 3(a) for the case when $\alpha = 1.4$. Application of a bias field field B_{zbias} strongly perturbs the trap. Increasing B_{zbias} from 0 to $0.72B_o$ shifts the trap center position $z_{\min}$ from $0.83R_1$ to $0.51R_1$. This permits precise adjustment of the position of an ultracold atom cloud and thereby control its interaction with the atom chip surface. The second effect of the bias field is to modify the trap shape. Figure 3(a) shows a symmetric trap is generated when $B_{\text{zbias}} = 0.72B_o$, where the magnetic field magnitude at the origin equals the field strength on the z-axis at $z_{\max} = 1.45R_1$. Atoms are then trapped if their temperature is less than

$$T_{\text{Trap}} = g_F m_F \mu_{\text{B}} B_{\text{Trap}}/k_{\text{B}}, \tag{7}$$

where k_{B} is Boltzmann's constant. B_{Trap} is defined as the smallest maximum field magnitude considering all possible directions from the trap center. For the trap illustrated in figure 3, the trap depth is largest for the symmetric trap and has the value $B_{\text{Trap}} = 1.075B_o$. A higher maximum trapping field is found when the field magnitude is plotted along other directions such as the radial direction as is shown in figure 4. It shows the magnetic field magnitude in the $x-z$ plane at $y = 0$ and the $x-y$ plane for $z_{\min} = 0.51R_1$ using a bias field $B_{\text{zbias}} = 0.72B_o$. A three dimensional trap is produced. For a ^{87}Rb atom in the ground state $|F = 2, m_F = 2\rangle$ hyperfine sublevel, a trap depth exceeding 0.5 mK is achieved if $R_1 = 60\ \mu$m using a current of 500 mA and $B_o = 8.33$ G. The dependence of the bias field that symmetrizes the trap along the z-direction and associated trap depth and center position, are plotted as a function of R_2/R_1 in figure 3(b).

The bias field can be readily generated using a large macroscopic coil that surrounds the entire atom chip apparatus. An alternative is to use different currents in the two microloops as shown in figure 1. Figure 5(a) shows the field produced along the z-axis for various values of I_2/I_1 in the absence of a macroscopic bias field. The trap has a symmetric shape when $I_2/I_1 = 1.23$. The dependence of the current ratio that symmetrizes the trap along the z-direction and associated trap depth and center position, are plotted as a function of R_2/R_1 in figure 5(b). An advantage of using different loop currents rather than a macroscopic bias field is that the center positions of neighbouring traps relative to the chip surface can be adjusted independently.

A limitation of magnetic traps having a zero field minimum is that atoms located near the trap center can undergo spin flips. These so called Majorana transitions limit the ultracold atom density. Traps were therefore developed having a nonzero field at the trap center to observe BEC [4]. One approach is to use an additional small coil, known as a Ioffe coil [34, 35] as shown in figure 1. Figure 6 shows the effect on the magnetic field of the double-loop trap due to an Ioffe coil having a radius $R_1/8$ centered at the position (1.4, 0, 0.15) R_1 and a current $I_{\text{IC}} = 9\ I_1$. The Ioffe coil shifts the trap center to position $(0.48, 0, 0.47)R_1$, where the field minimum is $0.104B_o$. The resulting trap is not symmetric and has a reduced trap depth of $0.48B_o$. The latter was obtained using the magnetic field at the saddle point shown at the lower right in figure 6(b) near the Ioffe coil.

Adjacent double-loop microtraps can be daisy chained together to create the microtrap array shown in figure 7(a). Here, each double-loop microtrap is composed of two loops having $R_2/R_1 = 2.2$ and is separated from neighbouring traps by a distance of $5R_1$. Figures 7(b)–(d) show the effect of the bias field $B_{\text{zbias}} = 1.62B_o$ on the field plotted in the x-, y- and z-directions. This field was numerically computed for the wire schematic shown in figure 7(a) that consists of a number of straight and circular arc wire segments. Each microtrap exerted only a small effect on its neighbour which can be seen in figure 7(d) where only the two end microtraps have a slightly different shape.

Figure 8 shows how atoms can be transferred between neighbouring microtraps. Here, two double-loop traps each having $R_2/R_1 = 1.4$ are considered whose centers are located at (0, 0, 0) and $(0.5, 0, -0.1)R_1$. The negative sign for the z position of the right trap means the microwires are embedded in the atom chip so as to avoid contacting and thereby shorting with the microwires of the left microtrap. Figure 8 shows the field magnitude in the $x-z$ plane as the current in the left (right) microtrap is decreased (increased). The resulting trap magnetic field is shifted but its shape is

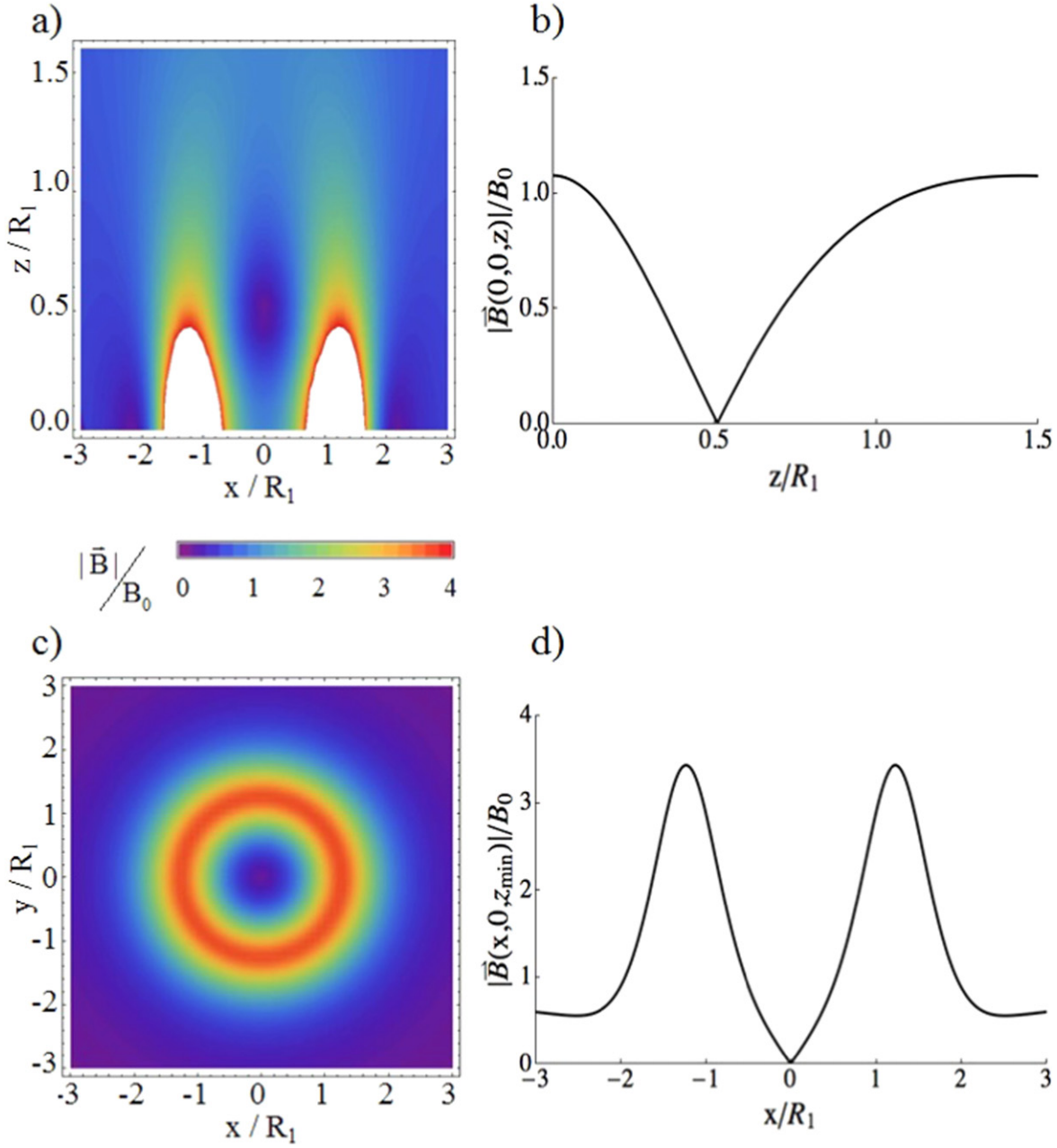

Figure 4. Spatial dependence of magnetic field when $R_2 = 1.4R_1$, $I_2 = I_1$ and $B_{\text{zbias}} = 0.72B_o$. (a) shows the magnetic field in the $x-z$ plane. (b) plots the magnetic field versus the distance z above the chip when $x = y = 0$. The trap has a minimum field at $z_{\min} = 0.51R_1$ (c) shows the magnetic field in the $x-y$ plane through the loop center when $z = z_{\min}$. (d) plots the field versus x when $y = 0$ and $z = z_{\min}$.

minimally perturbed. This is important to minimize loss of trapped atoms. Hence, it should be possible to transport atoms around a two-dimensional array using intermediate double-loop traps.

3. Experimental demonstration

Atom chips are fabricated employing similar lithographic techniques used to make computer chips [13]. Our latest atom chip was constructed using a 0.5 mm thick silicon wafer onto which a 100 nm silicon nitride insulating layer was deposited and then a 4 μm Cu layer [33]. The microwires were etched into the Cu surface where $R_1 = 60\,\mu$m. The microwire width was 7 μm. A 5 μm gap separated the wires from the Cu surface. The atom chip was mounted on a Cu heat sink. The atom chip assembly included a Rb dispenser which generated a rubidium vapour when a current was applied.

The mounted atom chip was encapsulated by a rectangular borosilicate glass cell whose outer wall was coated to reduce the reflectivity at 780 nm to less than 0.5% as illustrated in figure 9. The glass cell gave excellent optical access to a number of laser beams used to cool and probe the microtrapped atoms. A further reason to use a glass cell is that it is not magnetic unlike stainless steel and does not perturb the magnetic field. Various magnetic coils could be placed

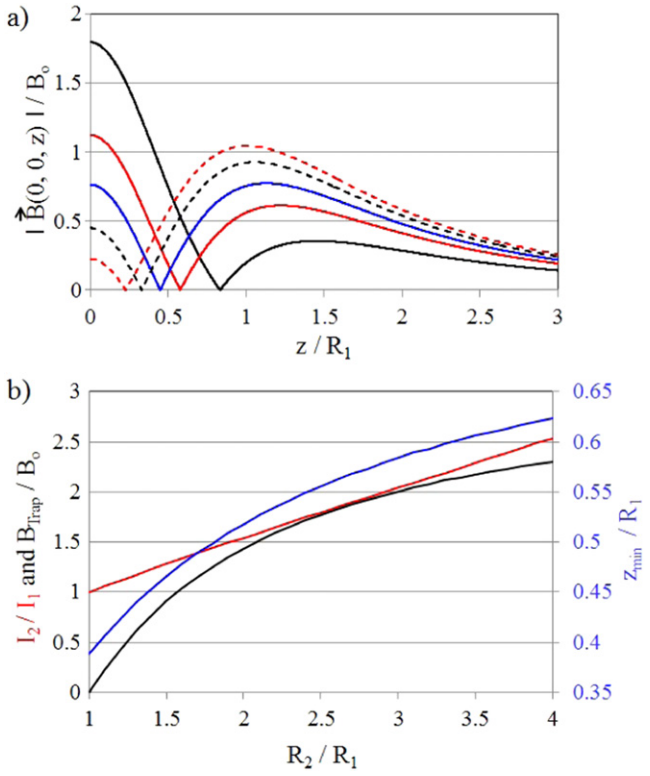

Figure 5. Double-loop microtrap without a bias field. (a) shows the magnitude of the magnetic field along the z-axis as a function of the distance z from the chip surface at $z = 0$ for the values I_2/I_1 of 1 (solid black), 1.15 (solid red), 1.23 (solid blue), 1.3 (black dash) and 1.35 (red dash) for the case when $R_2 = 1.4\ R_1$. (b) shows the dependence of I_2/I_1 (red) that symmetrizes the trap depth in the z-direction, the trap depth (black) and position of the microtrap along the z-axis (blue) as a function of R_2/R_1.

very close to the glass cell which facilitated generating fields of the requisite strength using a minimum of electric current.

The glass cell was mated to an ultra high vacuum chamber. This system was first pumped down using a turbo molecular pump and subsequently by an ion pump that also contained a titanium sublimation pump (TSP) located inside a cylindrical liquid nitrogen trap. The ion pump was located about 0.75 m from the glass cell to reduce stray magnetic fields at the atom chip to less than 0.5 G. Three additional pairs of Helmholtz coils then reduced the field at the atom chip to about 1 mG. The entire system was baked for over a week to remove impurities. The temperature was not allowed to exceed 120 °C to avoid thermal stress which might crack the glass as well as possibly damage the antireflection coating. A residual gas analyzer showed the pressure was due nearly entirely to hydrogen. Finally, the TSP was turned on and the pressure was reduced to below 1×10^{-10} torr which was the low end limit of the pressure gauge resolution.

Ultracold ^{87}Rb atoms suitable for loading microtraps are readily produced in a magneto-optical trap (MOT) using standard laser cooling techniques [36, 37]. Two coils generated the MOT quadrupole magnetic field having an axial gradient of 14 G cm^{-1} as illustrated in figure 9. The experiments used three independent laser systems. Each laser was frequency locked to a saturation absorption spectroscopy signal observed in a Rb vapour cell [33]. Acousto-optic modulators generated frequency shifted laser beams and also allowed precise control of the power and temporal sequence of the laser pulses. The trap laser frequency was detuned 14 MHz below the $F = 2 \rightarrow F' = 3$ cycling transition of the ^{87}Rb D2 line, where F and F' denote the hyperfine levels of the $5S_{1/2}$ ground state and $5P_{3/2}$ excited state, respectively. The trap laser intensity was 40 mW cm^{-2}. The repump laser was frequency locked to the $F = 1 \rightarrow F' = 2$ transition. Its intensity was 2 mW cm^{-2}. The transmission of the so called imaging laser beam through the ultracold atomic clouds was monitored using a CCD camera. The 50 μW imaging laser beam was directed in the x-direction. The MOT was populated with approximately 2×10^7 atoms in 6 s.

A challenge when transferring atoms from a MOT into a microtrap is that the microtrap volume is orders of magnitude smaller. A second problem is that the MOT proximity to the microtrap is limited by the atom chip which can block some of the MOT laser beams. The atom cloud generated by the MOT must be transported over distances of ≈1 cm with an accuracy of the microtrap size. This can be done by applying various magnetic fields to adjust the MOT position but is difficult to do without significant atom loss [30]. Another approach illustrated in figure 9 is to reflect laser beams from the atom chip surface to generate a surface MOT. The reflectivity of the Cu surface at 780 nm exceeded 90% [32]. Atoms can then be directly transferred from the surface MOT into the microtrap. An alternative is to transfer the atoms from the surface MOT into a far off resonance trap (FORT) created by focussing an infrared laser. This is especially useful when loading a microtrap array, where the FORT laser propagation direction is aligned with the one-dimensional array axis.

The first step to directly load atoms into the microtrap from the surface MOT was to physically compress the MOT (CMOT) by increasing the field gradient from 14 to 35 G cm^{-1} over a 50 ms time interval. Simultaneously, the trap laser detuning increased to 30 MHz while the repump laser intensity was cut in half to minimize atom heating. Next, all magnetic fields were turned off. The trap laser detuning increased to 50 MHz to facilitate polarization gradient cooling [36]. The MOT contained about 10^7 atoms after this 8 ms optical molasses stage. Next, over 90% of the atoms were optically pumped to the $|F = 2, m_F = 2\rangle$ magnetically trapped ground state Zeeman sublevel by a 1 ms circularly polarized 80 μW laser beam resonant with the $F = 2 \rightarrow F' = 2$ transition. Finally, the microtrap was turned on by abruptly ramping up the atom chip current to 0.5 A and the B_{zbias} field.

The microtrap array could be loaded from a FORT formed by focussing a 15 W laser beam operating at 1.06 μm. The infrared laser beam travelled in the y direction. The MOT cloud was compressed and atoms were cooled as previously described. The repump laser power was lowered to 40 μW while the CMOT and optical molasses stage durations were lengthened to 140 and 20 ms, respectively. This reduced spin exchange collisions that can cause a significant loss of trapped atoms [38, 39]. The FORT contained 7.5×10^5 atoms in the

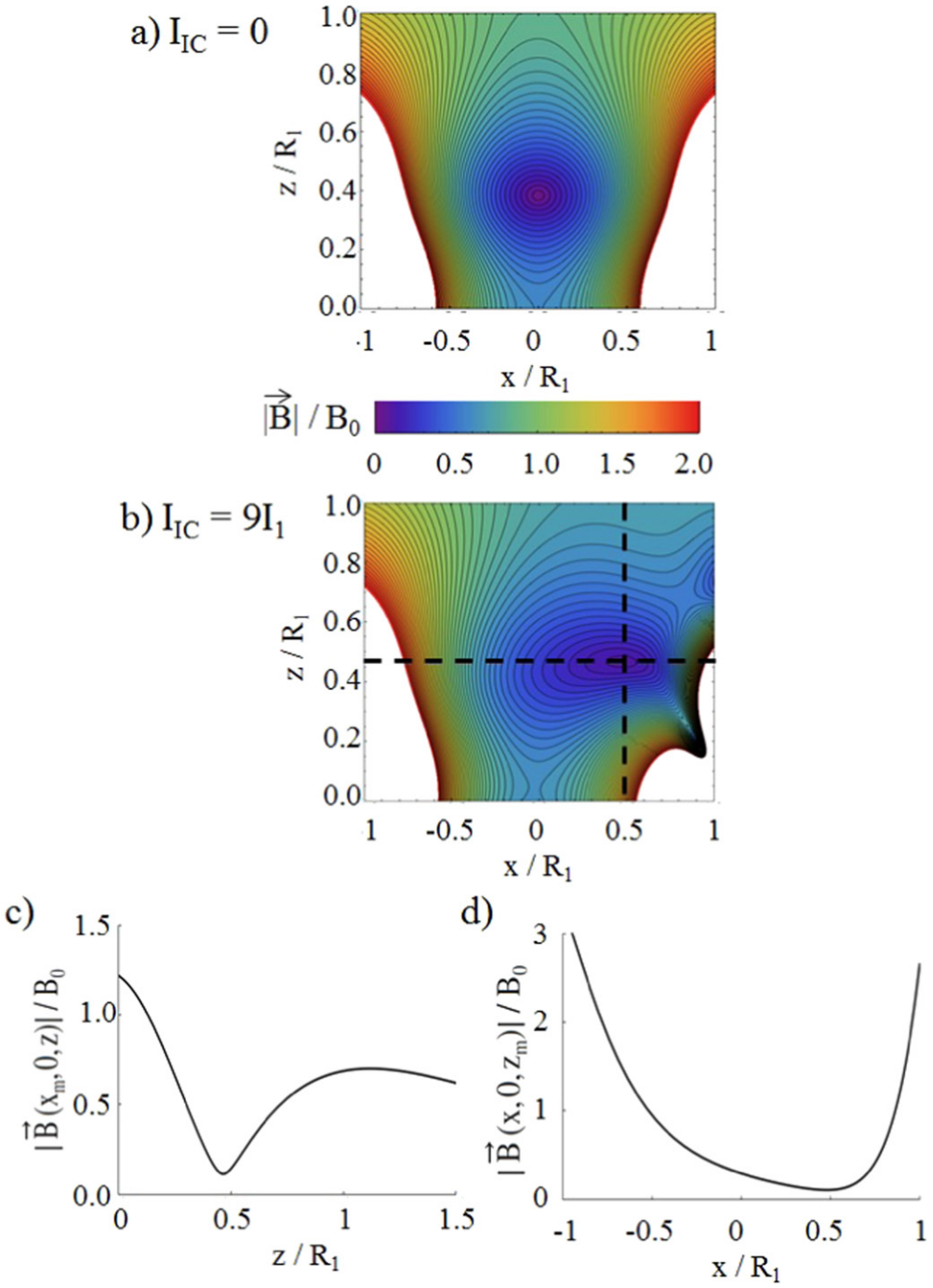

Figure 6. Effect of Ioffe coil current I_{IC} on the magnetic field in the $x-z$ plane. The Ioffe coil has a radius $R_1/8$ and is centered about the position $(1.4, 0, 0.15)R_1$ as illustrated in figure 1. The difference of adjacent contour lines corresponds to $0.04B_o$. (a) shows the magnetic field generated by only the double-loop microtrap having $R_2 = 1.4R_1$ and current $I_2 = 1.23I_1$. (b) shows the field when $I_{IC} = 9I_1$. (c) and (d) plot the field dependence along the z- and x-directions indicated by the dashed lines in (b).

$F = 1$ ground state hyperfine level as is shown in figure 10. The microtrap array was switched on over 20 ms by linearly increasing the bias magnetic field B_{zbias} and the atom chip current.

Atoms were kept in the microtrap array for as long as 400 ms before the arrival of a 50 μs imaging laser pulse. Variation of the probe delay time after the micotrap was switched off allowed the observation of the expansion of the atom cloud to obtain its temperature. The microtrapped atoms occupied the $|F = 1, m_F = -1\rangle$ ground state hyperfine sublevel in the case of FORT loading. The imaging laser was then superimposed with 100 μW of repump laser light to probe the atoms.

The number of microtrapped atoms loaded from the FORT is shown in figure 10. The microtrap populations were about equal except for the end traps located where the FORT cloud had fewer atoms. A similar atom number could be loaded into the array directly from the surface MOT.

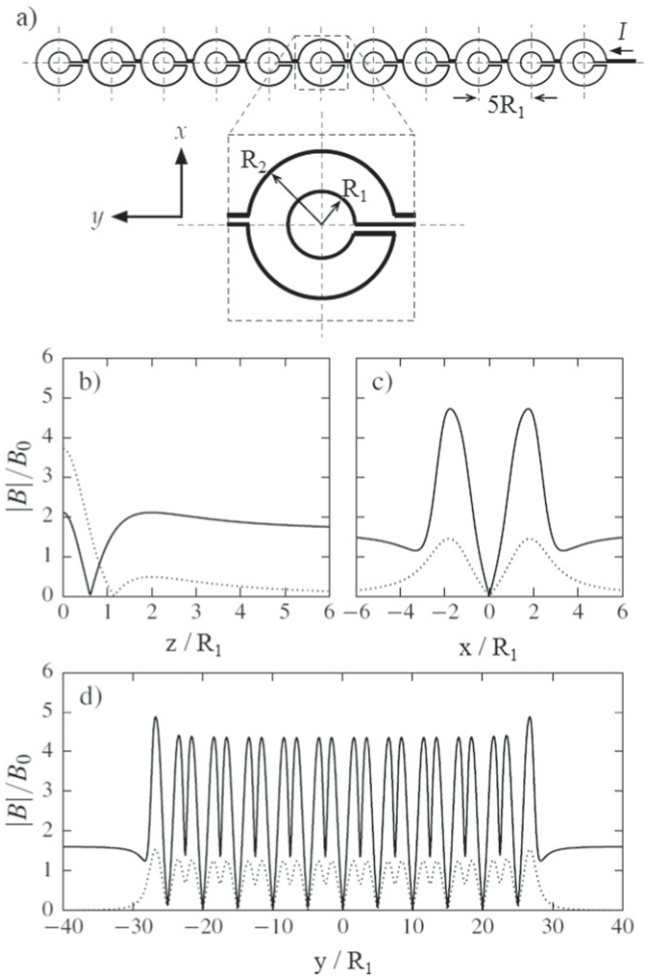

Figure 7. Linear array of 11 microtraps computed for $R_2 = 2.2R_1$ taken and reproduced with permission from [32]. Copyright IOP Publishing 2014. (a) shows the microwire pattern in the $x-y$ plane. (b)–(d) show the magnetic field dependence with (without) a bias field $B_{\text{zbias}} = 1.62B_o$ shown in solid black line (dashed black line) along the z-, x- and y-directions, respectively.

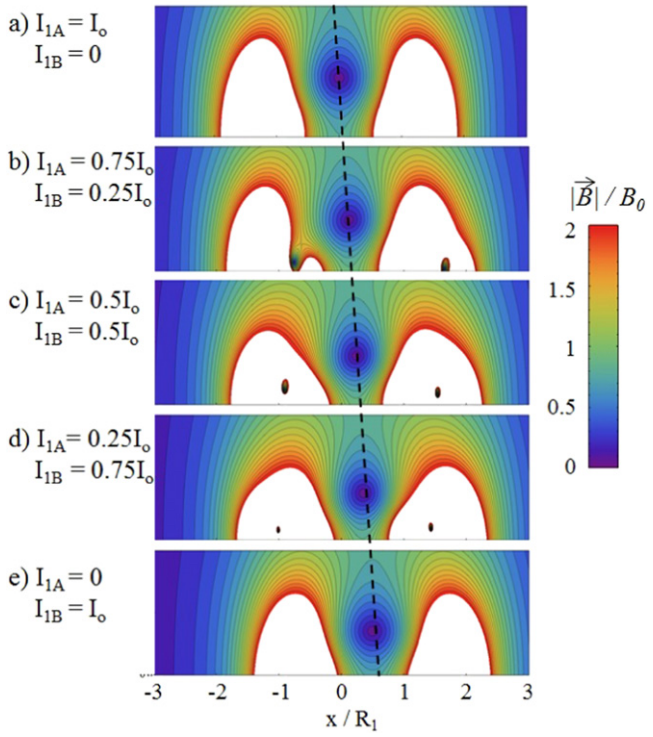

Figure 8. Magnetic field in the $x-z$ plane generated by microtrap A centered at (0,0,0) and microtrap B centered about the point embedded in the atom chip at $(0.5, 0, -0.1)R_1$. Each microtrap has $R_2 = 1.4R_1$ and is operated without a B_{zbias} field using current $I_2 = 1.23I_1$ where $I_1(I_2)$ is the current in the inner (outer) microloop. The difference of adjacent contour lines corresponds to $0.1B_o$. The field configurations in the $x-z$ plane are shown for the inner loop currents (a) $I_{1A} = I_o$, $I_{1B} = 0$, (b) $I_{1A} = 0.75I_o$, $I_{1B} = 0.25I_o$, (c) $I_{1A} = I_{1B} = 0.5I_o$, (d) $I_{1A} = 0.25I_o$, $I_{1B} = 0.75I_o$ and (e) $I_{1A} = 0$, $I_{1B} = I_o$. The vertical distance plotted in each figure is from $z = 0$ to $z = R_1$. The trap center is shifted as indicated by the dashed line.

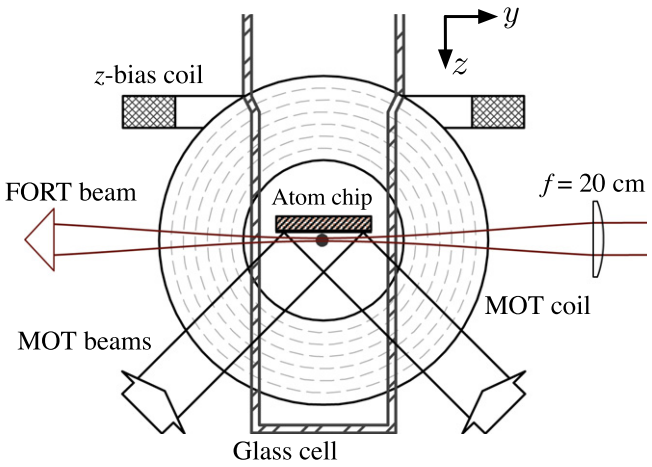

Figure 9. Apparatus used to load microtrap as is discussed in the text.

However, the atom cloud generated by the surface MOT is smaller than that of the FORT resulting in the populations of the left and right halves of the microtrap array differing by about a factor of two [32]. A temperature of $40 \pm 4\ \mu$K was observed for atoms loaded from the surface MOT while $11 \pm 2\ \mu$K was achieved using FORT loading. This lower temperature arises because evaporative cooling is facilitated at lower FORT laser power [40–42]. The microtrapped atom lifetime was 300 ± 22 ms. It was limited by collisions with background gas molecules [42] and Majorana transitions [2]. No change in pressure was observed even when the chip current was increased to 4 A. There was no evidence of microwire degradation at this elevated current.

Figure 11 shows the effect of the bias field on the number of atoms in a single microtrap having $R_1 = 300\ \mu$m and $R_2 = 660\ \mu$m. The bias field increased the trap depth as shown in figure 3 causing a dramatic increase in the trapped atom number. A bias field value of 8 G also optimized the overlap of the FORT and the microtrap. At higher fields, the microtrap position shifted toward the atom chip surface away from the FORT. Figure 11(b) shows the distance of the microtrapped atom cloud from the atom chip surface could be varied from 350 to 50 μm by adjusting B_{zbias}. The bias field also affected the smaller microtrap having $R_1 = 60\ \mu$m similarly. However, diffraction of the imaging laser makes it difficult to exactly measure the cloud position.

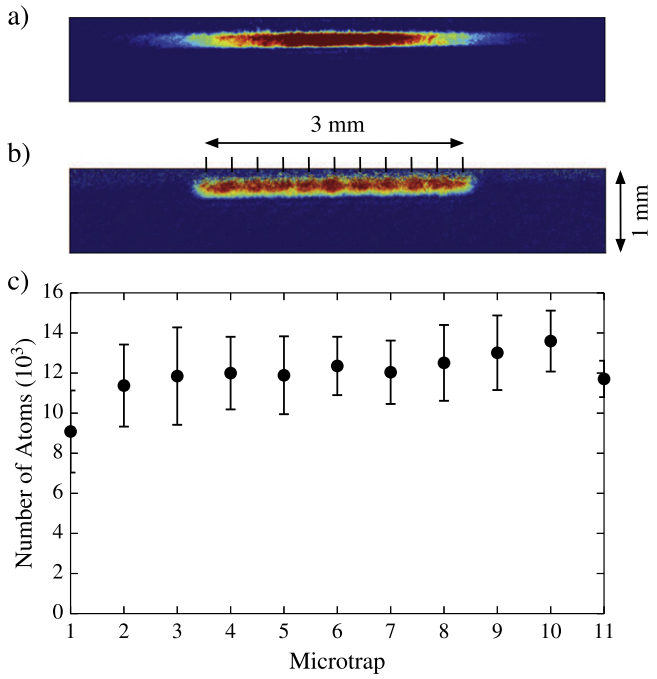

Figure 10. Transfer of atoms from FORT to microtrap array taken and reproduced with permission from [32]. Copyright IOP Publishing 2014. (a) Image of the atoms trapped in the FORT which was loaded from the surface MOT. The FORT was positioned 65 ± 15 μm beneath the atom chip surface. (b) Image of atoms in the microtrap array loaded using $B_{\mathrm{zbias}} = 3$ G from the FORT. The ticks on the top of (b) indicate the positions of the individual microtrap centers. (c) Number of atoms loaded into the individual microtraps counted from left to right.

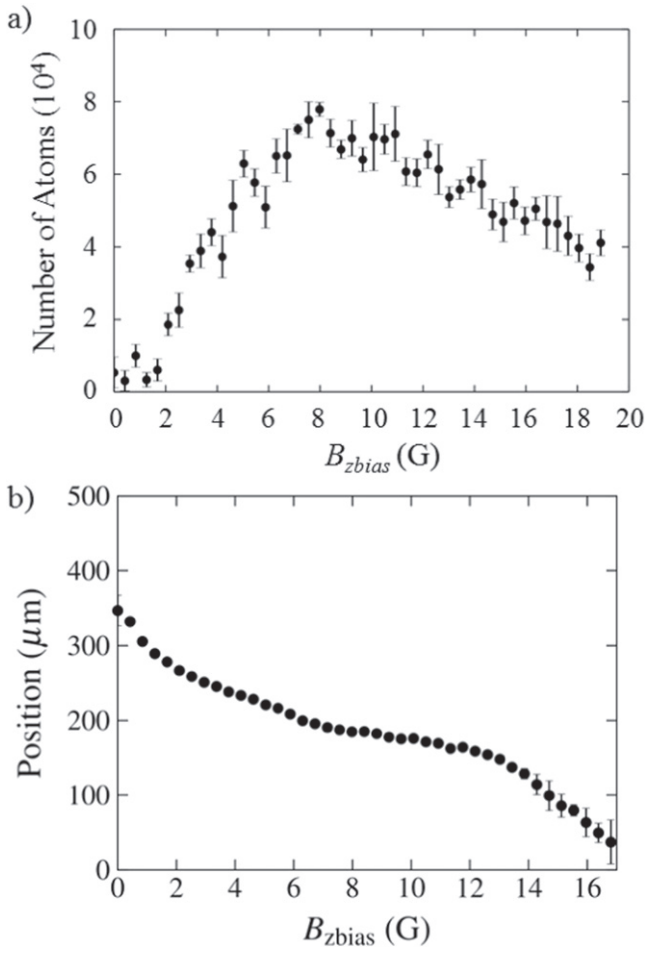

Figure 11. Effect of the B_{zbias} field on the (a) the number of atoms loaded into the microtrap and (b) the microtrap position taken and reproduced with permission from [31]. Copyright Springer 2013. This data was taken using a double-loop microtrap having $R_1 = 300$ μm, $R_2 = 660$ μm and $B_o = 8.33$ G.

4. Conclusions and future outlook

The double-loop microtrap has a simple design yet generates a versatile trap to study ultracold atoms. A similar number of atoms can be loaded into the microtrap either directly from a surface MOT or from a FORT. FORT loading is ideally suited for a linear microtrap array. A cylindrical lens would be needed to generate a sheet of FORT laser light for the case of a two-dimensional microtrap array. The FORT laser power can also be adjusted to facilitate evaporative cooling to control the atom temperature. The atom cloud position can be precisely adjusted by either applying a bias field perpendicular to the chip surface or using unequal currents in the two microwire loops. This is important when studying effects that depend strongly on the distance to the surface such as the Casimir–Polder interaction [43, 44]. A particularly useful feature of the double-loop microtrap when studying surface interactions is that the microwire loops do not perturb the atom chip surface immediately below the atom cloud. The double-loop microtrap generates a symmetric trap as shown in figure 3 located at a distance proportional to the inner loop radius above the atom chip surface. Embedding the double-loop microtrap in the atom chip would permit positioning the atom cloud arbitrarily close to the surface.

An interesting objective is to create an array where each microtrap has only a single atom. Collisional effects would then be absent which would improve the accuracy of atomic clocks/frequency standards compared to atomic vapour cell clocks [45]. An accuracy improvement of three orders of magnitude which equals the ratio of the Doppler width at room temperature compared to the natural transition linewidth could be expected as occurred with the development of a single trapped ion frequency standard [46]. The resulting apparatus would also be much more compact. Our work loaded $\approx 10^4$ (10^5) atoms into a single double-loop microtrap having $R_1 = 60$ (300) μm. The atom density was estimated using the observed atom temperature of 11 μK and the trap potential to be $\approx 1 \times 10^{11}$ atoms cm^{-3} in the smaller trap. The microtrap having $R_1 = 60$ μm used a current of 0.5 A and did not exhibit any degradation due to any resistive heating effects. The trap depth is proportional to the current divided by R_1. An order of magnitude smaller trap therefore requires ten times less current to achieve the same trap potential. Such a trap will require microwires having a smaller cross section which will increase the wire resistance. Resistive heating however will not increase as it depends on the square of the current times the electrical resistance of the microwires. A

smaller microtrap can be expected to have fewer atoms but a higher atom density limited by ultracold atom collisions and Majorana transitions [2]. These smaller numbers of atoms could be observed by detecting atomic fluorescence [47, 48].

Future possibilities include adding a micro Ioffe coil to generate a trap having a nonzero minimum field to avoid trap loss due to Majorana transitions. The small size of this Ioffe coil means that it does not obscure laser beams reflecting off the atom chip that create a surface MOT. Atoms could also be transported between array sites using intermediate double-loop microtraps. An advantage of the double-loop microtrap is that a photodiode or even a diode laser can be positioned on the atom chip above the ultracold atom cloud. This close proximity would simplify addressing individual microtraps which is critical for quantum computation. It would be an important step to the long term objective of creating a compact atom chip incorporating both the microtrap wires and the lasers. Hence, the double-loop microtrap is an invaluable tool for studying ultracold atoms.

Acknowledgments

The authors thank the Natural Science and Engineering Research Council of Canada for financial support. B Jian and A Mouraviev are the recipients of the York University Provost Scholarship and Research at York Award, respectively.

References

[1] Madison K W, Wang Y, Rey A M and Bongs K (ed) 2013 *Annual Review of Cold Atoms and Molecules* (Hackensack, NJ: World Scientific Publishing) **vol 1** pp 1–540
[2] Matthews M R, Wieman C E, Anderson M H, Ensher J R and Cornell E A 1995 *Science* **269** 198
[3] Davis K B, Mewes M O, Andrews M R, van Druten N J, Kurn D M and Ketterle W 1995 *Phys. Rev. Lett.* **75** 3969
[4] Pethick C J and Smith H 2008 *Bose–Einstein Condensation in Dilute Gases* (Cambridge: Cambridge University Press)
[5] DeMarco B and Jin D S 1999 *Science* **285** 1703
[6] Ludlow A D, Boyd M M, Ye J, Peik E and Schmidt P O 2015 *Rev. Mod. Phys.* **87** 637
[7] Wicht A, Hensley J M, Sarajlic E and Chu S 2002 *Phys. Scr.* **T102** 82
[8] Bouchendira R, Cladé P, Guellati-Khélifa S, Nez F and Biraben F 2001 *Phys. Rev. Lett.* **106** 080801
[9] Hanneke D, Fogwell S and Gabrielse G 2008 *Phys. Rev. Lett.* **100** 120801
[10] Schultz B E, Ming H, Noble G A and van Wijngaarden W A 2008 *Eur. Phys. J.* D **48** 171
[11] Safronova M S, Johnson W R and Derevianko A 1999 *Phys. Rev.* A **60** 4476
[12] Bergeman T, Erez G and Metcalf H J 1987 *Phys. Rev.* A **35** 1535
[13] Folman R, Krüger P, Schmiedmayer J, Denschlag J and Henkel C 2002 *Adv. At. Mol. Opt. Phys.* **48** 263
[14] Fortágh J and Zimmermann C 2007 *Rev. Mod. Phys.* **79** 235
[15] Hänsel W, Hommelhoff P, Hänsch T W and Reichel J 2001 *Nature* **413** 498
[16] Ott H, Fortágh J, Schlotterbeck G, Grossmann A and Zimmermann C 2001 *Phys. Rev. Lett.* **87** 230401
[17] Gierling M, Schneeweiss P, Visanescu G, Federsel P, Haffner M, Kern D P, Judd T E, Günther A and Fortágh J 2011 *Nat. Nanotechnol.* **6** 446
[18] Wang Y-J, Anderson D Z, Bright V M, Cornell E A, Diot Q, Kishimoto T, Prentiss M, Saravanan R A, Segal S R and Wu S 2005 *Phys. Rev. Lett.* **94** 090405
[19] Riedel M F, Böhi P, Li Y, Hänsch R W, Sinatra A and Treutlein P 2010 *Nature* **464** 1170
[20] Pritchard J D, Dinkelaker A N, Arnold A S, Griffin P F and Riis E 2012 *New J. Phys.* **14** 103047
[21] Arnold A S, Garvie C S and Riis E 2006 *Phys. Rev.* A **73** 041606
[22] Tejada J, Chudnovsky E M, del Barco E, Hernandez J M and Spiller T P 2001 *Nanotechnology* **12** 181
[23] Cirone M A, Negretti A, Calarco T, Krüger P and Schmiedmayer J 2005 *Eur. Phys. J.* D **35** 165
[24] Birkl G and Fortagh J 2007 *Laser Photonics Rev.* **1** 12
[25] Lester B J, Luick N, Kaufman A M, Reynolds C M and Regal C A 2015 *Phys. Rev. Lett.* **115** 073003
[26] Knoernschild C, Zhang X L, Isenhower L, Gill A T, Lu F P, Saffman M and Kim J 2010 *Appl. Phys. Lett.* **97** 134101
[27] Lichtman M, Piotrowicz M, Xia T, Isenhower L and Saffman M 2014 *24th Int. Conf. on Atomic Physics* p 319
[28] Leung V Y F *et al* 2014 *Rev. Sci. Instrum.* **85** 053102
[29] Jose S, Surendran P, Wang Y, Herrera I, Krzemien L, Whitlock S, McLean R, Sidorov A and Hannaford P 2014 *Phys. Rev.* A **89** 051602(R)
[30] Jian B and van Wijngaarden W A 2013 *J. Opt. Soc. Am.* B **30** 238
[31] Jian B and van Wijngaarden W A 2014 *Appl. Phys.* B **115** 61
[32] Jian B and van Wijngaarden W A 2014 *J. Phys. B: At. Mol. Opt. Phys.* **47** 215301
[33] Jian B 2014 *PhD Thesis* York University
[34] Gott V, Ioffe M S and Tel'kovskii V G 1962 *Nucl. Fusion* **3** (Suppl.) 1045
[35] Pritchard D E 1983 *Phys. Rev. Lett.* **51** 1336
[36] Metcalf H J and van der Straten P 1999 *Laser Cooling and Trapping* (New York: Springer)
[37] Lu B and van Wijngaarden W A 2004 *Can. J. Phys.* **82** 81
[38] Kuppens S J M, Corwin K L, Miller K W, Chupp T E and Wieman C E 2000 *Phys. Rev.* A **62** 013406
[39] Walker T and Feng P 1997 *Adv. At. Mol. Opt. Phys.* **34** 125
[40] Adams C S, Lee H J, Davidson N, Kasevich M and Chu S 1995 *Phys. Rev. Lett.* **74** 3577
[41] Cano D, Hattermann H, Kasch B, Zimmermann C, Kleiner R, Koelle D and Fortágh J 2011 *Eur. Phys. J.* D **63** 17
[42] van Dongen J, Hu Z, Clement D, Dufour G, Booth J L and Madison K W 2011 *Phys. Rev.* A **84** 022708
[43] Lamoreaux S K 1997 *Phys. Rev. Lett.* **78** 5
[44] Obrecht J M, Wild R J, Antezza M, Pitaevskii L P, Stringari S and Cornell E A 2007 *Phys. Rev. Lett.* **98** 063201
[45] Camparo J 2007 *Phys. Today* **98** 33
[46] Madej A A, Dube P, Zhou Z, Bernard J E and Gertsvolf M 2012 *Phys. Rev. Lett.* **109** 203002
[47] Teper I, Lin Y-J and Vuletić V 2006 *Phys. Rev. Lett.* **97** 023002
[48] Ockeloen C F, Tauschinsky A F, Spreeuw R J C and Whitlock S 2010 *Phys. Rev.* A **82** 061606